Robotica (2018) volume 36, pp. 925–944. © Cambridge University Press 2018
doi:10.1017/S0263574718000140

Heel-strike and toe-off motions optimization for humanoid robots equipped with active toe joints

Majid Sadedel†, Aghil Yousefi-Koma†*, Majid Khadiv‡ and Faezeh Iranmanesh†

† *Center of Advanced Systems and Technologies (CAST), School of Mechanical Engineering, College of Engineering, University of Tehran, Tehran, Iran*
‡ *Center of Excellence in Robotics and Control, Advanced Robotics & Automated Systems (ARAS) Lab, Department of Mechanical Engineering, K. N. Toosi University of Technology, Tehran, Iran*

(Accepted January 31, 2018. First published online: March 8, 2018)

SUMMARY
In this paper, a walking pattern optimization procedure is implemented to yield the optimal heel-strike and toe-off motions for different goal functions. To this end, first, a full dynamic model of a humanoid robot equipped with active toe joints is developed. This model consists of two parts: multi-body dynamics of the robot which is obtained by Lagrange and Kane methods and power transmission dynamic model which is developed using system identification approach. Then, a gait planning routine is presented and consistent parameters are specified. Several simulations and experimental tests are carried out on SURENA III humanoid robot which is designed and fabricated at the Center of Advanced Systems and Technologies located in the University of Tehran. Afterward, a genetic algorithm optimization is adopted to compute the optimal walking patterns for five different goal functions including energy consumption, stability margin, joint velocity, joint torque and required friction coefficient. Also, several parametric analyses are performed to characterize the effects of heel-strike and toe-off angle and toe link mass and length on these five goal functions. Finally, it is concluded that walking pattern without heel-strike and toe-off motions requires less friction coefficient than the pattern with heel-strike and toe-off motions. Also, heavier toe link lowers tip-over instability and slippage occurrence possibility, but requires more energy consumption and joint torque.

KEYWORDS: Active toe joint; Gait optimization; Heel-strike motion; Toe-off motion; Genetic algorithm.

1. Introduction

Two important phases of a humanoid robot gait are heel-strike and toe-off motions. These phases play a major role in developing human-like walking patterns, so several researches have been conducted in this field. Chevallereau compared and optimized different types of walking patterns with foot rotation for a 2D[1] and 3D[2] humanoid robot. Also, Grizzle studied the stability of gaits with foot rotation using Poincare return map.[3]

To have more natural toe-off motion, some robots are equipped with toe joints. For instance, H7,[4] Lola,[5] Toyota[6] and HRP-4C[7] have active toe joints, while Wabian[8] has passive toe joints. Some advantages of using active toe joints are faster walking,[4] step height augmentation,[4,9] stability enhancement,[10,11] energy saving,[12] maximum joint velocity reduction[10] and resemblance to human gait.[7,10] Handhura developed walking pattern with stretched knee motion using active toe and heel joints.[13] Also, Kouchaki investigated standing balance control of a biped robot with active toe joints.[14]

On the other hand, passive toe joints are studied in humanoid field as well and faster and smoother walking is reported as an advantage.[8,15] Kajita developed a running pattern for HRP-2LT equipped

* Corresponding author. E-mail: aykoma@ut.ac.ir

https://doi.org/10.1017/S0263574718000140 Published online by Cambridge University Press

with toe springs.[16] Moreover, Kumar introduced hybrid toe joint which is an active toe joint with a spring and damper mechanism, to reduce the maximum required torque for this joint.[17]

According to the aforementioned studies, an optimization process may be carried out in order to obtain the best toe joint design and effective heel-strike and toe-off motions. There are few goal functions mentioned in the literature such as minimum energy consumption[18–22] and minimum required joint torque.[19,23,24] Also, most of the optimization parameters are mainly related to the pelvis motion. However, it seems crucial to take heel and toe parameters into account as design variables during optimization process. Therefore, in this paper, our main interest is optimization of four foot-related parameters including heel-strike and toe-off angles and toe link mass and length. Five different goal functions are considered during optimization process such as minimum energy consumption, maximum stability margin, minimum joint torque, minimum joint velocity and minimum friction coefficient.

In this paper, first, a dynamic model of a 3D humanoid robot is presented. In some studies, Lagrange method has been adopted to model the multi-body dynamics of humanoid robots.[1,4,25–29] Some other researches exploited Newton–Euler approach for this purpose.[30–33] Also, power transmission system was considered ideal in most of these studies. However, in this study, and for the sake of generating an accurate dynamic model, a combination of Lagrange and system identification approaches is used. Lagrange method is adopted for modeling of the non-linear and phase-dependent dynamic behaviors of the multi-body robot. System identification approach is used to simplify the complexity of modeling of the power transmission system components. Finally, total required joint torque which is the summation of these two model outputs is obtained.

The next step is walking pattern generation. All different methods for this step can be categorized into two groups: online methods in which patterns are calculated while robot is walking and offline approach in which robot follows previously defined commands. Since walking pattern generation is real-time in online path planning approach, a simplified model is used to describe the dynamic behaviors of the humanoid robot. Inverted pendulum model,[34] cart table model,[35] two-mass model[36] and three-mass model[37] have been introduced in the literature. On the other hand, full multi-body dynamics of the robot is basically used in offline methods.[38] In this paper, for the sake of accurate optimization, offline path planning approach is chosen.

Finally, an optimization procedure based on GA is adopted to determine the optimal walking pattern for different goal functions. Unlike other studies that only focus on hip motion, in this paper, the main concentrations are on the foot rotation and toe joint design parameters. Therefore, several parametric analyses are carried out to determine the effect of heel-strike and toe-off angles and toe link design parameters such as mass and length on five different goal functions including minimum energy consumption, maximum stability margin, minimum joint torque, minimum joint velocity and minimum friction coefficient.

Main novelties in this study are as follows:

- Using a hybrid dynamic model consisting of a multi-body dynamics method and power transmission system identification approach to achieve a more accurate dynamic model for the optimization procedure.
- Using some novel goal functions such as maximum stability margin, minimum joint velocity and minimum required friction coefficient.
- Investigation on the effects of changing foot rotation and toe joint design parameters on different goal functions.

2. Dynamic Modeling

The understudy humanoid robot has 14 DoF in its lower body (3 DoF for each hip, 1 DoF for each knee, 2 DoF for each ankle and finally 1 DoF for each toe). The upper body is assumed to be rigid and fixed during motions. Figure 1 illustrates the scheme of this humanoid robot. Moreover, mass and geometric properties of the robot are specified in Table I based on SURENA III humanoid robot. It should be mentioned that SURENA III does not have toe joints, currently. Therefore, the toe properties are hypothetical.

https://doi.org/10.1017/S0263574718000140 Published online by Cambridge University Press

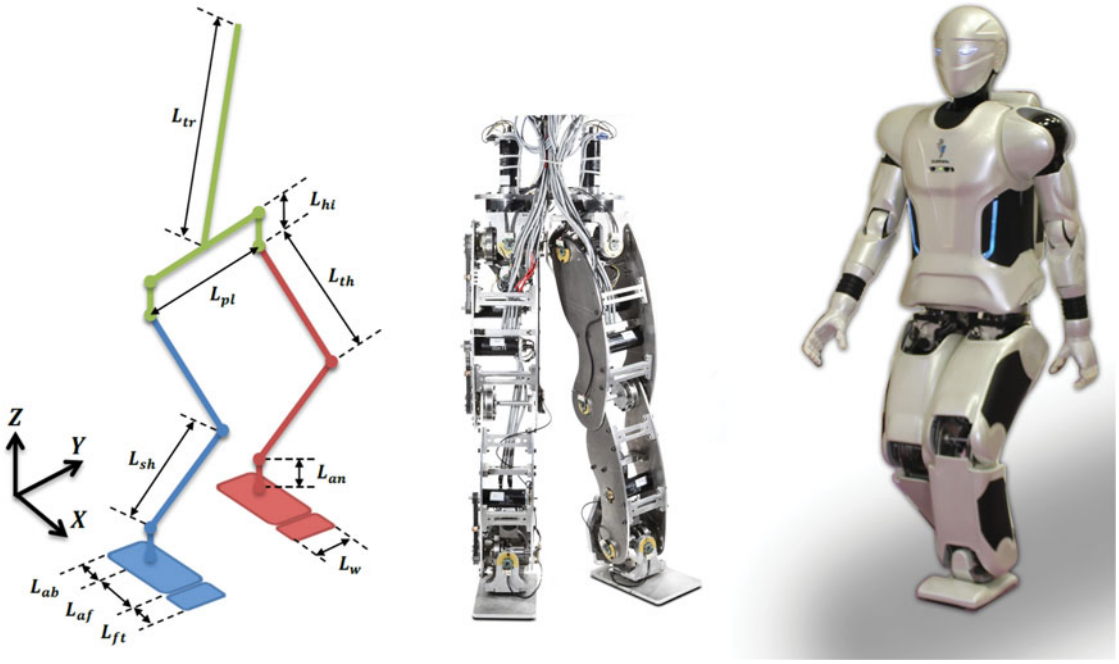


Fig. 1. Scheme of understudy humanoid robot based on SURENA III.

Table I. Mass and geometric properties of understudy humanoid robot.

Parameters	L_{tr}	L_{pl}	L_{hi}	L_{th}	L_{sh}	L_{an}	L_{ab}	L_{af}	L_w	L_{ft}
Length (mm)	568	230	114.5	360	360	128	101.5	166.5	190	30

Parameters	M_{trunk}	M_{pelvis}	$M_{\text{hip universal}}$	M_{thigh}	M_{shank}	$M_{\text{ankle universal}}$	M_{foot}	M_{toe}
Mass (Kg)	39.396	4.088	2.706	6.327	4.561	2.236	3.859	0.500

Rest of this section explains full dynamic model of a humanoid robot with an active toe joint.

2.1. Multi-body dynamic model

Motions of the humanoid robot are described using generalized coordinate vector which can be written as follows:

$$\begin{aligned} q &= \begin{bmatrix} q_r & q_l & q_{pl} \end{bmatrix}^T \\ q_r &= \begin{bmatrix} q_{hx} & q_{hy} & q_{hz} & q_{ky} & q_{ax} & q_{ay} & q_{ty} \end{bmatrix} \\ q_l &= \begin{bmatrix} q_{hx} & q_{hy} & q_{hz} & q_{ky} & q_{ax} & q_{ay} & q_{ty} \end{bmatrix} \\ q_{pl} &= \begin{bmatrix} X_{pl} & Y_{pl} & Z_{pl} & \alpha_{pl} & \beta_{pl} & \gamma_{pl} \end{bmatrix} \end{aligned} \tag{1}$$

where q_r and q_l denote the joint angles of right and left leg, respectively. Also, q_{pl} specifies the position and the orientation of the pelvis in the global coordinate system.

Dynamic model of the robot can be stated in the following form using Lagrange or Kane method:

$$M_{20\times20}(q)\,\ddot{q}_{20\times1} + V_{20\times1}(q,\dot{q}) + G_{20\times1}(q) = Q_{20\times1} \tag{2}$$

where $M(q)$ is the symmetric positive inertia matrix, $V(q,\dot{q})$ contains the centrifugal and Coriolis terms, $G(q)$ stands for the gravitational forces and Q denotes the vector of the generalized force. Robot is considered without any interaction with the environment at first. In this case, just the joint

https://doi.org/10.1017/S0263574718000140 Published online by Cambridge University Press

torques act on the robot. Therefore, the generalized force vector can be stated as

$$\begin{aligned} Q_{20\times1} &= B_{20\times14}\tau_{14\times1} \\ B_{20\times14} &= \begin{bmatrix} I_{14\times14} \\ 0_{6\times14} \end{bmatrix} \\ \tau_{14\times1} &= \begin{bmatrix} \tau^r_{7\times1} \\ \tau^l_{7\times1} \end{bmatrix} \end{aligned} \tag{3}$$

Then, interactions between robot foot and the ground can be considered as holonomic constraints. Each constraint may be replaced by an appropriate force or torque using constraint relaxation method.[39] The acting positions of these forces and torques change between sole and toe based on the ZMP[40] position and walking phase during motion. Therefore, corresponding terms in the generalized force vector are phase-dependent. These terms may be stated as given in Table II for different situations. It should be noted that Table II does not indicate the walking phases sequentially.

According to Table II, if ZMP point is located under the sole of the front stance foot, the ground reactions are supposed to act on the "s point" which is in the middle of the sole link. In this case, no ground reactions act on the toe link and active toe joint tolerates the weight of toe link. Conversely, if ZMP point is placed under the toe of the front stance foot, the ground reactions are assumed to apply on the "t point" which is in the middle of the toe link and no ground reaction would act on the "s point".

According to the foot contact with the ground, the location of "s point" and "t point" on the sole and toe links are fixed with respect to the ground in any direction. This can be considered as three contact constraints. Moreover, sole and toe links cannot rotate around the "s point" and "t point" either which gives us three more constraints. These six constraints can be replaced by three forces and three torques as ground reactions. These ground reactions turn up in generalized force vector in the form of $J^T_{(20\times6)}F_{(6\times1)}$, where J is the Jacobian matrix of the ground reaction point with respect to the global coordinate system.

The location of "h point" at the heel is fixed with respect to the ground, but the sole link can rotate freely around the "h point" in Y direction. These constraints can be replaced by three forces and two torques in X and Z directions. These ground reactions turn up in the generalized force vector in the form of $J^T_{(20\times5)}F_{(5\times1)}$. Since there are no constraints for rotation in Y direction, M_y does not appear in ground reactions, and thus, the corresponding line in the Jacobian matrix is omitted.

Joint torques, ground reactions, generalized coordinates and its first and second derivatives are the parameters of the Eq. (2). According to Eq. (2), all unknown parameters including joint torques and ground reactions are on right-hand side of the equation. Given the walking pattern, the generalized coordinates and its derivatives can be determined. By substituting these parameters, Eq. (2) yields a set of linear equations.

The number of equations is the same as the number of elements in the generalized coordinates (i.e. 20). According to Table II, number of unknowns is phase-dependent (i.e. 20, 25 and 26). If number of unknowns is the same as number of equations (i.e. 20), the Gaussian elimination method[41] is employed, since it is efficient from both execution time and numerical accuracy standpoints. If the number of unknowns is greater than the number of equations (i.e. 25 or 26), there are infinitely many solutions, all of which can be written in the following form using the Moore–Penrose pseudo-inverse method:[42]

$$AX = B \Rightarrow X = A^{\dagger}B + \left(I - A^{\dagger}A\right)k \tag{4}$$

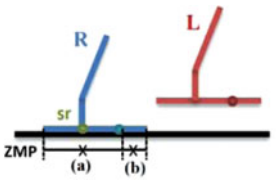
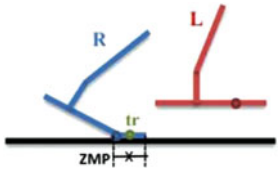
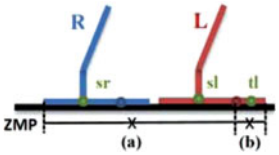
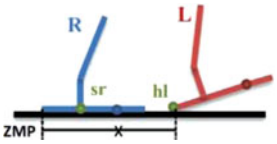
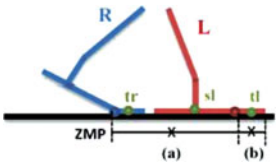
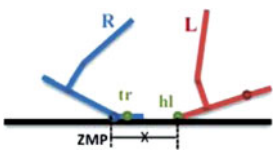
where $A^{\dagger}$ represents Moore–Penrose pseudo-inverse of matrix A, I is the identity matrix and k is an arbitrary constant vector.

Two subsets of these solution sets are our area of interest in this study:

- $X = A^{\dagger}B$ in which quadratic norm of X is smaller than the norm of any other solution.
- X which is calculated based on Gaussian elimination and has the fewest possible non-zero components.

https://doi.org/10.1017/S0263574718000140 Published online by Cambridge University Press

Table II. Generalized force vector during different walking phases.

Case	Motion phase	Schema	Ground reactions and Q
1	Single support (SS) with right sole		$F_{sr} = [F_{x_r}, F_{y_r}, F_{z_r}, M_{x_r}, M_{y_r}, M_{z_r}]^T$ *a)* $Q = [B \quad J_{sr}^T]_{20\times 20}\begin{bmatrix}\tau \\ F_{sr}\end{bmatrix}_{20\times 1}$ $F_{tr} = [F_{x_r}, F_{y_r}, F_{z_r}, M_{x_r}, M_{y_r}, M_{z_r}]^T$ *b)* $Q = [B \quad J_{tr}^T]_{20\times 20}\begin{bmatrix}\tau \\ F_{tr}\end{bmatrix}_{20\times 1}$
2	SS with right toe		$F_{tr} = [F_{x_r}, F_{y_r}, F_{z_r}, M_{x_r}, M_{y_r}, M_{z_r}]^T$ $Q = [B \quad J_{tr}^T]_{20\times 20}\begin{bmatrix}\tau \\ F_{tr}\end{bmatrix}_{20\times 1}$
3	Double support (DS) with both soles		*a)* $F_{sr} = [F_{x_r}, F_{y_r}, F_{z_r}, M_{x_r}, M_{y_r}, M_{z_r}]^T$ $F_{sl} = [F_{x_l}, F_{y_l}, F_{z_l}, M_{x_l}, M_{y_l}, M_{z_l}]^T$ $Q = [B \quad J_{sr}^T \quad J_{sl}^T]_{20\times 26}\begin{bmatrix}\tau \\ F_{sr} \\ F_{sl}\end{bmatrix}_{26\times 1}$ $F_{sr} = [F_{x_r}, F_{y_r}, F_{z_r}, M_{x_r}, M_{y_r}, M_{z_r}]^T$ $F_{tl} = [F_{x_l}, F_{y_l}, F_{z_l}, M_{x_l}, M_{y_l}, M_{z_l}]^T$ *b)* $Q = [B \quad J_{sr}^T \quad J_{tl}^T]_{20\times 26}\begin{bmatrix}\tau \\ F_{sr} \\ F_{tl}\end{bmatrix}_{26\times 1}$
4	DS with right sole and left heel		$F_{sr} = [F_{x_r}, F_{y_r}, F_{z_r}, M_{x_r}, M_{y_r}, M_{z_r}]^T$ $F_{hl} = [F_{x_l}, F_{y_l}, F_{z_l}, M_{x_l}, M_{z_l}]^T$ $Q = [B \quad J_{sr}^T \quad J_{hl}^T]_{20\times 25}\begin{bmatrix}\tau \\ F_{sr} \\ F_{hl}\end{bmatrix}_{25\times 1}$
5	DS with right toe and left sole		$F_{tr} = [F_{x_r}, F_{y_r}, F_{z_r}, M_{x_r}, M_{y_r}, M_{z_r}]^T$ $F_{sl} = [F_{x_l}, F_{y_l}, F_{z_l}, M_{x_l}, M_{y_l}, M_{z_l}]^T$ *a)* *b)* $Q = [B \quad J_{tr}^T \quad J_{sl}^T]_{20\times 26}\begin{bmatrix}\tau \\ F_{tr} \\ F_{sl}\end{bmatrix}_{26\times 1}$ $F_{tr} = [F_{x_r}, F_{y_r}, F_{z_r}, M_{x_r}, M_{y_r}, M_{z_r}]^T$ $F_{tl} = [F_{x_l}, F_{y_l}, F_{z_l}, M_{x_l}, M_{y_l}, M_{z_l}]^T$ $Q = [B \quad J_{tr}^T \quad J_{tl}^T]_{20\times 26}\begin{bmatrix}\tau \\ F_{tr} \\ F_{tl}\end{bmatrix}_{26\times 1}$
6	DS with right toe and left heel		$F_{tr} = [F_{x_r}, F_{y_r}, F_{z_r}, M_{x_r}, M_{y_r}, M_{z_r}]^T$ $F_{hl} = [F_{x_l}, F_{y_l}, F_{z_l}, M_{x_l}, M_{z_l}]^T$ $Q = [B \quad J_{tr}^T \quad J_{hl}^T]_{20\times 25}\begin{bmatrix}\tau \\ F_{tr} \\ F_{hl}\end{bmatrix}_{25\times 1}$

https://doi.org/10.1017/S0263574718000140 Published online by Cambridge University Press

The second solution set yields some zero ground reaction components which is not compatible with the reality. Therefore, the pseudo-inverse method is chosen.

2.2. Power transmission dynamic model

Unlike multi-body dynamic model of robot, power transmission dynamic is not phase-dependent. To simplify the complexity of modeling different components of power transmission system, system identification method is exploited. The aim of this section is to obtain a simple model for the power transmission system, using linear identification method. This model computes motor current (which linearly corresponds to joint torque) through joint states (i.e. $\theta, \dot{\theta}, \ddot{\theta}$) in the load side. In Fig. 2, system identification test bench for the power transmission system is illustrated.

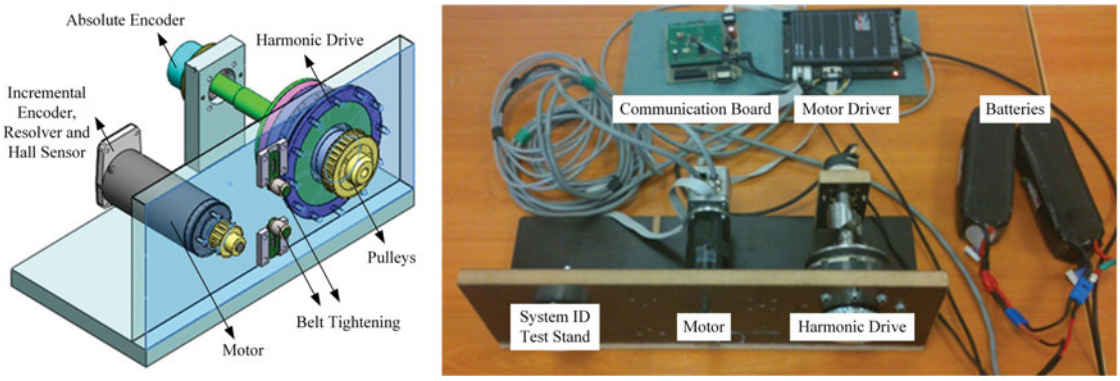


Fig. 2. System identification test bench for the power transmission system.

The power transmission system for each joint of SURENA III humanoid robot consists of these elements: Maxon EC motor, timing belts and pulleys with a gear ratio of 1:2, belt tightening and harmonic drive with a gear ratio of 1:160. Each EC motor has an incremental encoder, resolver and hall sensor. Moreover, each joint has an absolute encoder.

Knee joint trajectories for various robot velocities are commanded to the driver and then motor current (I) is measured. A simple model is considered for the motor current at first and the results are compared with the experimental motor current (I_{exp}). The model error is computed using the following equation:

$$\text{Error} = \frac{1}{T}\int_{t=0}^{T} \left| I_{\text{exp}} - I \right| \mathrm{d}t \tag{5}$$

Afterwards, by adding feasible terms, the optimum system identification model with minimum error is calculated. After carrying out lots of trials and errors, the best model for the power transmission system was obtained as follows:

$$I = J\ddot{\theta} + C\dot{\theta} + Bsgn\left(\dot{\theta}\right) \tag{6}$$

where I is motor current, $\dot{\theta}$ is joint velocity, $\ddot{\theta}$ is joint acceleration, J is effective inertia, C is viscous friction coefficient and B is Coulomb friction coefficient.

The tests are repeated using knee trajectories for different gait velocities and the standard deviation and consistency measure of model parameters are calculated (Table III) using the following formula:[43]

$$\begin{aligned} \bar{x} &= \tfrac{\sum x_i}{N} \\ S &= \sqrt{\tfrac{\sum (x_i - \bar{x})^2}{N}} \\ C &= \tfrac{S}{\bar{x}} \end{aligned} \tag{7}$$

where x_i is a calculated coefficient for each test, N is the number of tests and $\bar{x}$, S and C are average, standard deviation and consistency measure of that coefficient, respectively.

https://doi.org/10.1017/S0263574718000140 Published online by Cambridge University Press

Table III. Standard deviation and consistency measure of the model parameters.

Velocity (km/hr)	Error (amp)	J (amp.s^2)	C (amp.s)	B (amp)
0.2	0.889	0.996	8.378	2.611
0.3	0.991	0.924	6.642	2.892
0.4	0.929	0.111	6.459	2.856
0.5	1.633	1.232	3.579	2.753
0.6	1.519	0.555	4.546	2.780
0.7	1.517	0.901	2.643	3.220
Average		**0.787**	**5.375**	**2.852**
Standard Deviation		**0.396**	**2.153**	**0.205**
Consistency Measure		**50.34%**	**40.05%**	**7.19%**

As it may be seen, model parameters are consistent for various experiments since the consistency measure is less than 80%.

To sum up, the joint torques can be calculated as follows:

$$\begin{aligned} \tau_{\text{total}} &= \tau_{\text{Multi-body model}} + K_i I_{\text{Motor}} \\ I_{\text{Motor}} &= J\ddot{\theta} + C\dot{\theta} + Bsgn\left(\dot{\theta}\right) \end{aligned} \tag{8}$$

where K_i is the motor torque constant.

3. Gait Optimization

In this section, a path planning method for a 3D humanoid robot gait with active toe joints is presented. Afterwards, optimization parameters and different goal functions are introduced. At the end, GA method is adopted to optimize walking pattern parameters.

3.1. Path planning

This path planning routine is based on the position (X, Y and Z) of the ankle and hip joint and the orientation (roll, pitch and yaw) of the foot and pelvis link in the task space. The description of path planning parameters is presented in Table IV. Also, visual representations of path planning parameters in the sagittal and coronal planes are depicted in Figs. 3 and 4, respectively. Each cycle of the gait is consisting of a DS and SS phases. According to Table IV, If $T_{dm1} = 0$ and $T_{dm2} = T_d$, then there is

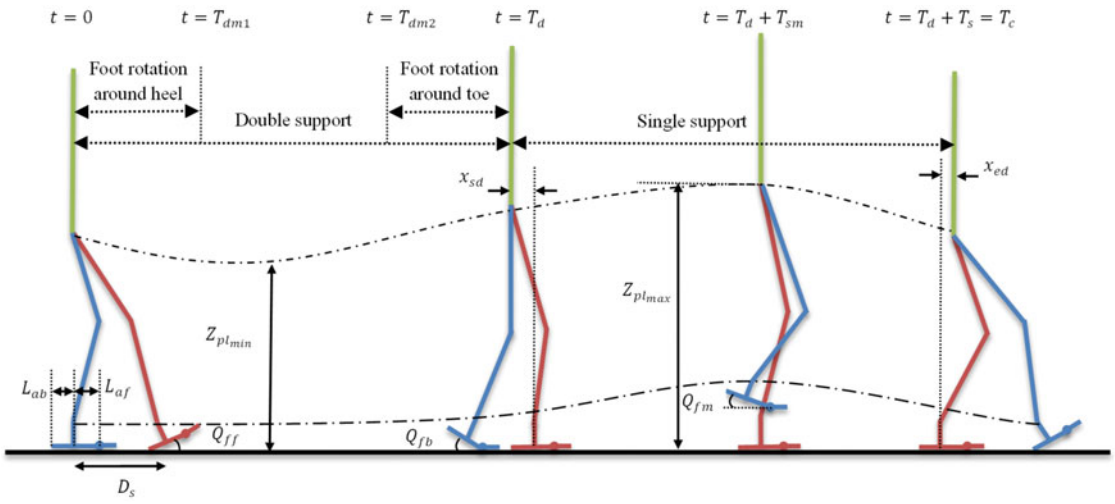


Fig. 3. Visual representation of path planning parameters in the sagittal plane.

https://doi.org/10.1017/S0263574718000140 Published online by Cambridge University Press

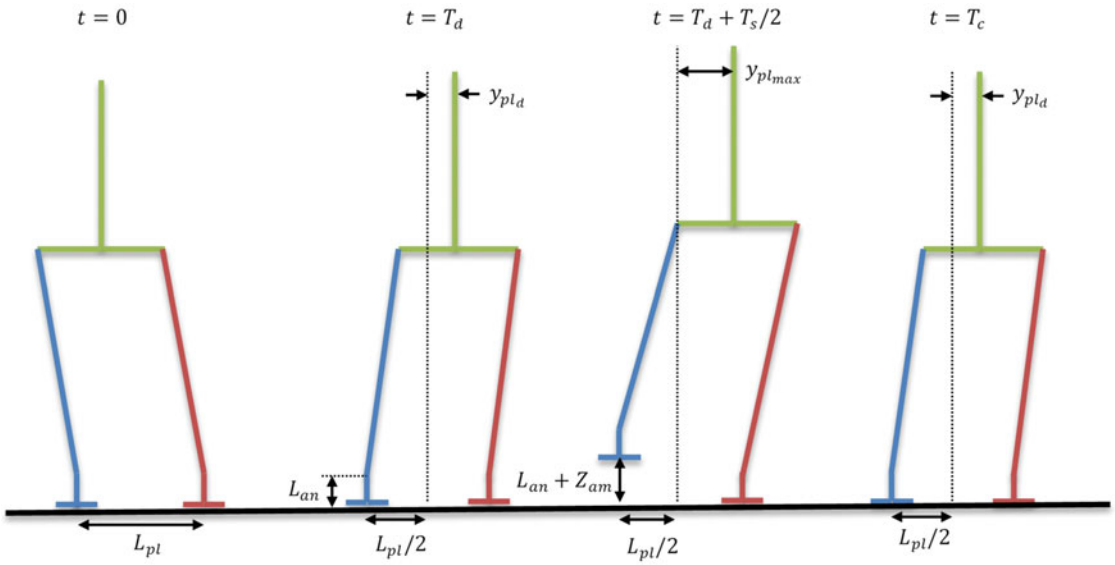


Fig. 4. Visual representation of the path planning parameters in the coronal plane.

Table IV. Path planning parameters and the corresponding values.

Parameters	Value	Dimension	Description
V	0.7	km/h	Walking velocity of the robot
D_c	0.4	m	Stride length
T_c	D_c/V	s	Walking cycle time
T_d	$0.4T_c$	s	DS time
T_s	$T_c - T_d$	s	SS time
T_{sm}	$0.4T_s$	s	Middle time in SS in which the position of ankle in Z direction is maximum
T_{dm1}	$0.3T_d$	s	First middle time in DS in which the heel-strike motion ends
T_{dm2}	$0.7T_d$	s	Second middle time in DS in which the toe-off motion starts
Z_{am}	0.05	m	Position of ankle in Z direction at T_{sm}
Q_{fm}	0	deg	Angle of swing foot with respect to the ground at T_{sm}
Q_{fb}	10	deg	Angle of toe rotation at the end of DS
Q_{ff}	-10	deg	Angle of heel rotation at the start of DS
X_{ed}	$0.15D_c$	m	Distance of the pelvis and stance ankle in X direction at the end of SS
X_{sd}	$0.1D_c$	m	Distance of the pelvis and stance ankle in X direction at the start of SS
$Y_{pl_{\max}}$	$0.6L_{pl}$	m	Position of pelvis in Y direction at the middle of SS which is maximum
Y_{pl_d}	$0.5L_{pl}$	m	Position of pelvis in Y direction at the start of DS
$Z_{pl_{\max}}$	$0.9L_{pl}$	m	Position of pelvis in Z direction at the middle of SS which is maximum
$Z_{pl_{\min}}$	$0.87L_{pl}$	m	Position of pelvis in Z direction at the middle of DS which is minimum

https://doi.org/10.1017/S0263574718000140 Published online by Cambridge University Press

no foot rotation around toe or heel in DS. In this regard, the whole DS phase is like Table II, Case 3. If $0 < T_{dm1} < T_{dm2} < T_d$, then the DS phase is a sequence of Table II, Cases 4, 3 and 5. On the other hand, if $0 < T_{dm2} < T_{dm1} < T_d$, then the DS phase is a sequence of Table II, Cases 4, 6 and 5. Using this technique, different types of walking pattern are achievable. It should be noted that the feet reaches the ground with zero velocity and acceleration. Therefore, there is no impact in the transition phase.

According to Fig. 3, pitch orientation of right foot (β_{fr}) has the following constraints:

$$\beta_{fr} = \begin{cases} 0 & 0 \le t \le T_{dm2} \\ Q_{fb} & t = T_d \\ Q_{fm} & t = T_d + T_{sm} \\ Q_{ff} & t = T_c \\ 0 & T_c + T_{dm1} \le t \le 2T_c \end{cases} \tag{9}$$

To have smooth trajectory with velocity and acceleration continuity, four spline curves with the order of 5, 4, 4 and 5 are generated, respectively.

Moreover, the position of right ankle in X and Z directions has these constraints:

$$x_{ar} = \begin{cases} 0 & 0 \le t \le T_{dm2} \\ L_{af}\left(1 - \cos\left(Q_{fr}\right)\right) + L_{an}\sin\left(Q_{fr}\right) & t = T_d \\ 2D_c + L_{ab}\left(\cos\left(Q_{fr}\right) - 1\right) + L_{an}\sin\left(Q_{fr}\right) & t = T_c \\ 2D_c & T_c + T_{dm1} \le t \le 2T_c \end{cases} \tag{10}$$

Three spline curves with the order of 5 are generated too.

$$z_{ar} = \begin{cases} L_{an} & 0 \le t \le T_{dm2} \\ L_{af}\sin\left(Q_{fr}\right) + L_{an}\cos\left(Q_{fr}\right) & t = T_d \\ L_{an} + Z_{am} & t = T_d + T_{sm} \\ -L_{ab}\sin\left(Q_{fr}\right) + L_{an}\cos\left(Q_{fr}\right) & t = T_c \\ L_{an} & T_c + T_{dm1} \le t \le 2T_c \end{cases} \tag{11}$$

All four spline curve are also with the order of 5.

The trajectories of X, Y and Z position of pelvis have these constraints:

$$x_p = \begin{cases} x_{ed} & t = 0 \\ D_c - x_{sd} & t = T_d \\ D_c + x_{ed} & t = T_c \\ 2D_c - x_{sd} & t = T_c + T_d \\ 2D_c + x_{ed} & t = 2T_c \end{cases} \tag{12}$$

https://doi.org/10.1017/S0263574718000140 Published online by Cambridge University Press

Four spline curves with the order of 3 are generated.

$$y_p = \begin{cases} -Y_{pl_d} & t = 0 \\ Y_{pl_d} & t = T_d \\ Y_{pl_{\max}} & t = T_d + T_s/2 \\ Y_{pl_d} & t = T_c \\ -Y_{pl_d} & t = T_c + T_d \\ -Y_{pl_{\max}} & t = T_c + T_d + T_s/2 \\ -Y_{pl_d} & t = 2T_c \end{cases} \tag{13}$$

The order of spline trajectories are 3, 4, 4, 3, 4 and 4, respectively.

$$z_p = \begin{cases} Z_{pl_{\min}} & t = T_d/2 \\ Z_{pl_{\max}} & t = T_d + T_s/2 \\ Z_{pl_{\min}} & t = T_c + T_d/2 \\ Z_{pl_{\max}} & t = T_c + T_d + T_s/2 \end{cases} \tag{14}$$

All three spline curve are with the order of 5.

It should be noted that the distance between the ankle joints in the lateral direction is considered to be constant (L_{pl}) in order to avoid self-collision of the legs (Fig. 4). Although, adding an inequality constraint is sufficient to avoid self-collision phenomenon, a constant distance is chosen to simplify the gait planning routine. Moreover, to gain simplicity, roll and yaw orientations of the feet and roll, pitch and yaw orientations of the pelvis are assumed to be constant too.

After generating these trajectories in task space, the trajectories in joint space are calculated using inverse kinematics.[44] It should be considered that there is kinematic redundancy in each leg due to the presence of active toe joint extra DoF. Therefore, additional trajectory for the angle of active toe joint is needed with the following constraints:

$$\theta_t = \begin{cases} 0 & 0 \le t \le T_{dm2} \\ -Q_{fb} & t = T_d \\ 0 & t = T_c \end{cases} \tag{15}$$

Two spline curves with the order of 5 are generated for the angle of active toe joint.

Using this method, all joint angle trajectories are determined for a walking pattern with heel-strike and toe-off motions for a 3D humanoid robot with an active toe joint.

3.2. GA optimization

In this section, the optimization procedure based on GA is presented. According to Table IV, the optimization parameters are D_c, T_d, T_{sm}, T_{dm1}, T_{dm2}, Q_{fb}, Q_{ff}, X_{ed}, X_{sd}, $Y_{pl_{\max}}$, Y_{pl_d}, $Z_{pl_{\max}}$ and $Z_{pl_{\min}}$. Five negative goal functions are chosen to optimize these walking pattern parameters. Positive values are reserved for non-feasible motions. GA algorithm is exploited to find the minimum value of the goal functions. These optimization goal functions are as follows:

- Minimum energy consumption:

$$J = -\frac{1}{\sum_{i=1}^{14} E_i} \tag{16}$$

where E_i is the energy consumption of joint i per walking distance.

https://doi.org/10.1017/S0263574718000140 Published online by Cambridge University Press

- Maximum stability:

$$J = \max\left(SM_x, SM_y\right) \tag{17}$$

where SM_x and SM_y are the stability margins, which are the minimum distance between ZMP point and the support polygon bounds in X and Y directions. Negative SM indicates stable motion according to ZMP criterion while non-negative SM means possibility of tip-over.

- Minimum joint velocity:

$$J = -\frac{1}{\max\limits_{i=1:14} |\dot{\theta}|_{\max_i}} \tag{18}$$

where $\dot{\theta}_{\max_i}$ is maximum velocity of joint i.

- Minimum joint torque:

$$J = -\frac{1}{\max\limits_{i=1:14} |\tau|_{\max_i}} \tag{19}$$

where $\tau_{\max_i}$ is maximum required torque of joint i.

- Minimum friction coefficient:

$$J = -\frac{1}{\mu} \tag{20}$$

where μ is the required friction coefficient to avoid slippage during walking which can be computed as

$$\mu = \max_{0 \le t \le 2T_c} \frac{\sqrt{\left(\sum F_x\right)^2 + \left(\sum F_y\right)^2}}{\sum F_z} \tag{21}$$

where $\sum F_x$, $\sum F_y$ and $\sum F_z$ are total ground reaction force in X, Y and Z directions, respectively.

In order to avoid infeasible motions, some constraints are taken into account. If walking pattern does not meet these constraints, then goal function will be considered to be a large positive number. The constraints are as follows:

- Stability constraint: If ZMP reaches the support polygon bound, then the motion will be unstable.

$$\left.\begin{array}{l} SM_x > 0 \\ SM_y > 0 \end{array}\right\} \Rightarrow J \gg 0 \tag{22}$$

- Actuator constraint: If the maximum required joint torque or velocity is beyond the actuator limit, then the motion will be infeasible.

$$\left.\begin{array}{l} \max\limits_{i=1:14} \dot{\theta}_{\max_i} > \max \dot{\theta}_{\text{actuator}} \\ \max\limits_{i=1:14} \tau_{\max_i} > \max \dot{\tau}_{\text{actuator}} \end{array}\right\} \Rightarrow J \gg 0 \tag{23}$$

- Singularity constraint: If knee joint angle approaches zero, then near singularity condition will occur which leads to high knee joint velocities.

$$\theta_{\text{knee}} < \theta_{\text{threshold}} \Rightarrow J \gg 0 \tag{24}$$

https://doi.org/10.1017/S0263574718000140 Published online by Cambridge University Press

- Joint range of motion (RoM) constraint: According to robot design restriction, there are some joint RoM limits especially in the hip joint.

$$\left.\begin{array}{l}\theta_i < \theta_i^{\min} \\ \theta_i > \theta_i^{\max}\end{array}\right\} \Rightarrow J \gg 0; \quad i = 1:14 \tag{25}$$

- Foot and ground collision constraint: All points of the feet must lie above the ground level.

$$Z_{\text{foot}} < 0 \Rightarrow J \gg 0 \tag{26}$$

4. Example of Optimal Motion

In this section, the kinematic and dynamic model calculation of a 0.7 Km/h gait which is optimized to have the maximum stability is presented. Moreover, several simulations are presented to indicate these calculations.

4.1. Kinematic model results

To indicate the kinematic model results of the humanoid robot, a snapshot of simulation of the walking cycle with the initiation and termination phases is illustrated in Fig. 5.

4.2. Analytical dynamic model results

Two test methods are performed to check the calculation of the developed analytical dynamic model. In the first one, the LHS of the Eq. (2) is determined using both Lagrange and Kane methods. Then,

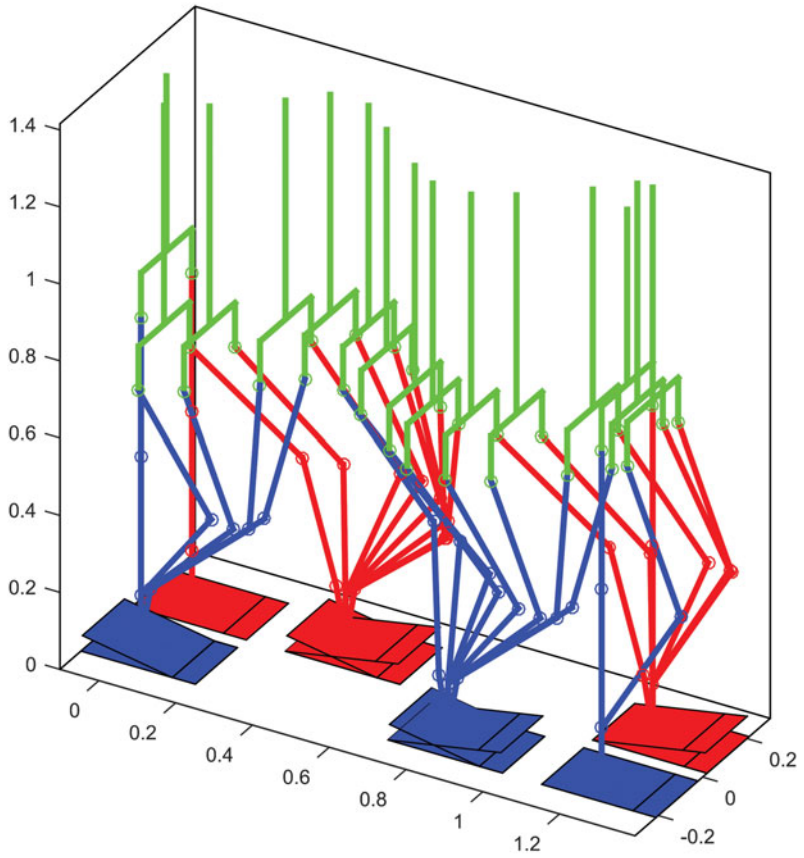


Fig. 5. A snapshot of one walking cycle with the start and stop phases.

https://doi.org/10.1017/S0263574718000140 Published online by Cambridge University Press

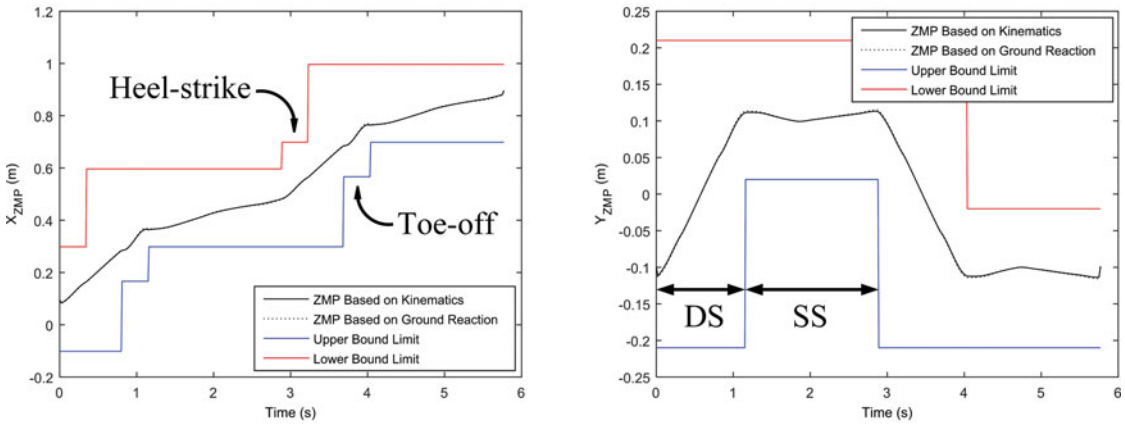


Fig. 6. ZMP point based on the robot kinematics and the ground reactions.

by substituting an arbitrary set of generalized coordinates and its first- and second-order derivatives into both equations, the calculation of the LHS of the Eq. (2) is confirmed.

In the second method, ZMP is calculated based on the robot kinematics (Eq. (27)[45]) and the ground reactions (Eq. (28)) and then compared.

$$\begin{aligned} X_{\text{ZMP}} &= \frac{\sum_{i=1}^{n} x_{G_i} \times m_i\left(\ddot{z}_{G_i}+g\right) - \sum_{i=1}^{n} z_{G_i} \times m_i \ddot{x}_{G_i} - \sum_{i=1}^{n} \bar{I}_{y_i} \ddot{q}_{y_i}}{\sum_{i=1}^{n} m_i\left(\ddot{z}_{G_i}+g\right)} \\ Y_{\text{ZMP}} &= \frac{\sum_{i=1}^{n} y_{G_i} \times m_i\left(\ddot{z}_{G_i}+g\right) - \sum_{i=1}^{n} z_{G_i} \times m_i \ddot{y}_{G_i} - \sum_{i=1}^{n} \bar{I}_{x_i} \ddot{q}_{y_i}}{\sum_{i=1}^{n} m_i\left(\ddot{z}_{G_i}+g\right)} \end{aligned} \tag{27}$$

$$\begin{aligned} X_{\text{ZMP}} &= \frac{F_{z_r} X_r + F_{z_l} X_l - M_{y_r} - M_{y_l}}{F_{z_r} + F_{z_l}} \\ Y_{\text{ZMP}} &= \frac{F_{z_r} Y_r + F_{z_l} Y_l - M_{x_r} - M_{x_l}}{F_{z_r} + F_{z_l}} \end{aligned} \tag{28}$$

where F and M are ground force and torque reactions which are applied in $[X \quad Y]^T$ with respect to feet coordinate systems origins. According to Fig. 6, ZMPs that are calculated based on both methods are coincident. The upper and lower limits for the ZMP shows the border of support polygon in X and Y directions. These limits depend on the walking phase, foot location and the sole link dimensions.

4.3. Experimental results

A 0.7 Km/h walking pattern with the maximum stability is implemented on SURENA III humanoid robot. It was mentioned that SURENA III does not have toe joints, yet. Hence, to make the presented method compatible with the robot, toe link mass and length are considered to be zero.

Center of mass and ZMP point which is calculated using six axis force/torque sensor mounted on robot feet are depicted in Fig. 7. Also, joint torque and energy consumption of the right foot based on the presented dynamic model and motor current are illustrated in Figs. 8 and 9, respectively. Moreover, Fig. 9 shows energy consumption of each walking phase. It can be seen that the results of presented dynamic model and the experimental tests are consistent. Energy consumption of the knee joint has the maximum error of 12%, which can be due to several reasons including

- parameter errors such as link mass, moment of inertia and length,
- joint following errors,
- power transmission identification errors.

5. Optimization and Parametric Analysis

In this section, the results obtained from optimization procedures and parametric analyses are presented. Generally, five mentioned goal functions have these main effects on walking pattern:

https://doi.org/10.1017/S0263574718000140 Published online by Cambridge University Press

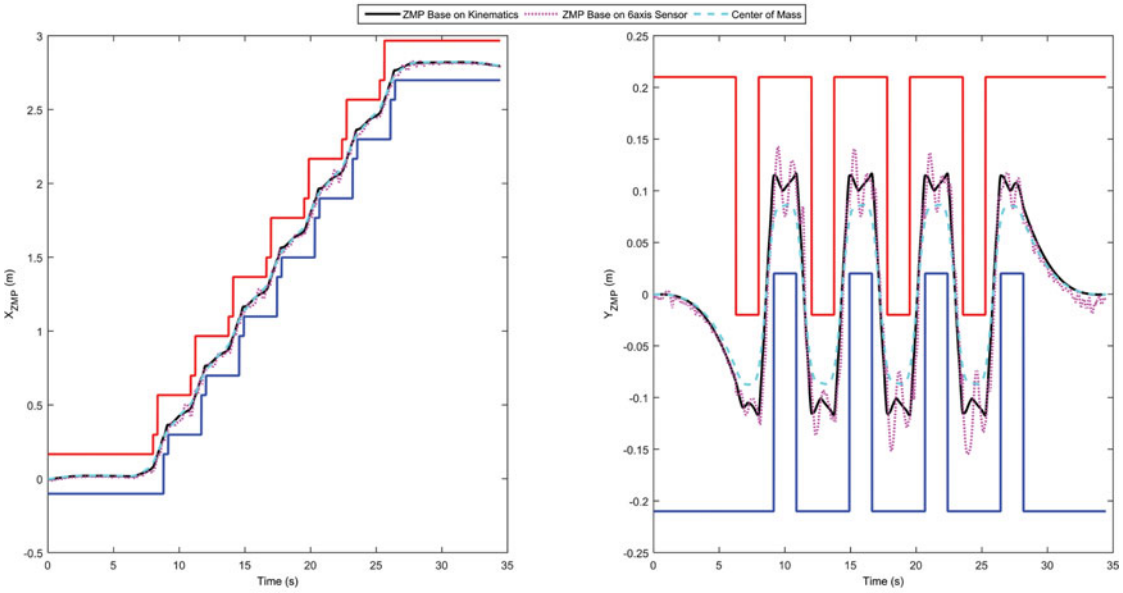


Fig. 7. Center of mass and ZMP point based on the presented dynamic model and six axis sensor.

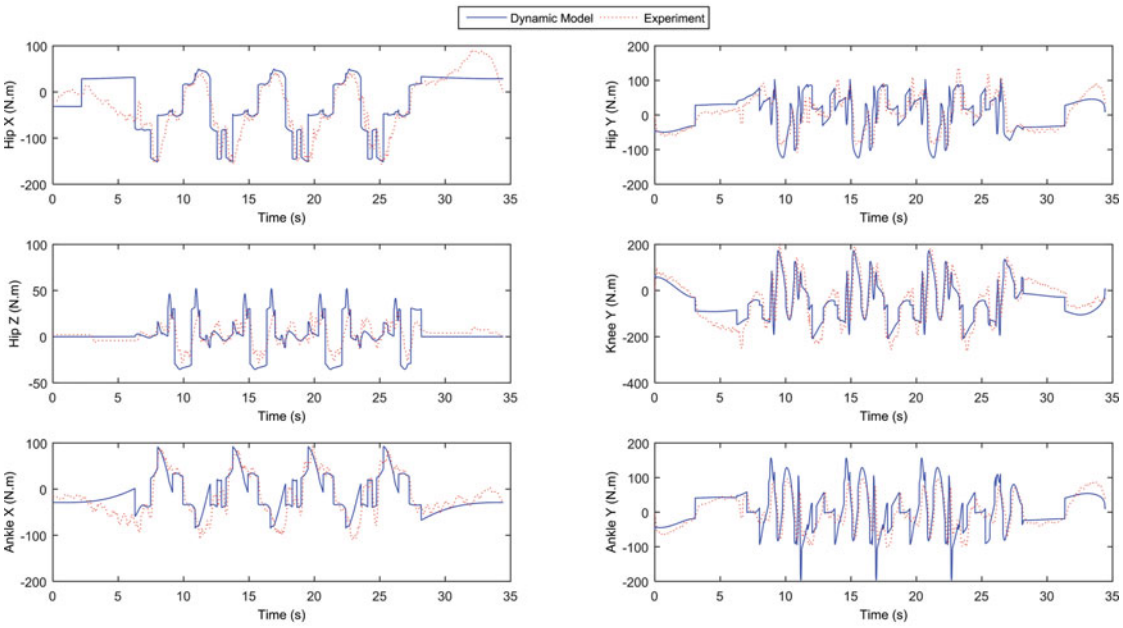


Fig. 8. Joint torques of right foot based on the presented dynamic model and motor current.

- Adopting "minimum energy consumption" and "minimum joint torque" goal functions leads to human-like walking pattern with knee stretched to reduce knee joint torque and energy consumption.
- On the other hand, using "minimum joint velocity" and "maximum stability" goal functions force knee joint to bend more to avoid near singularity condition.
- Finally, adopting "minimum friction coefficient" goal function leads to a smooth pelvis path planning with the minimum acceleration.

In Fig. 10, optimization results for the five goal functions are illustrated with respect to robot motion velocity. Each subplot depicts one of the goal functions for the five optimization procedures. For instance, first subplot shows that the walking pattern which is optimized to have maximum stability, consumes more energy than the others. On the other hand, it is obvious that the walking

https://doi.org/10.1017/S0263574718000140 Published online by Cambridge University Press

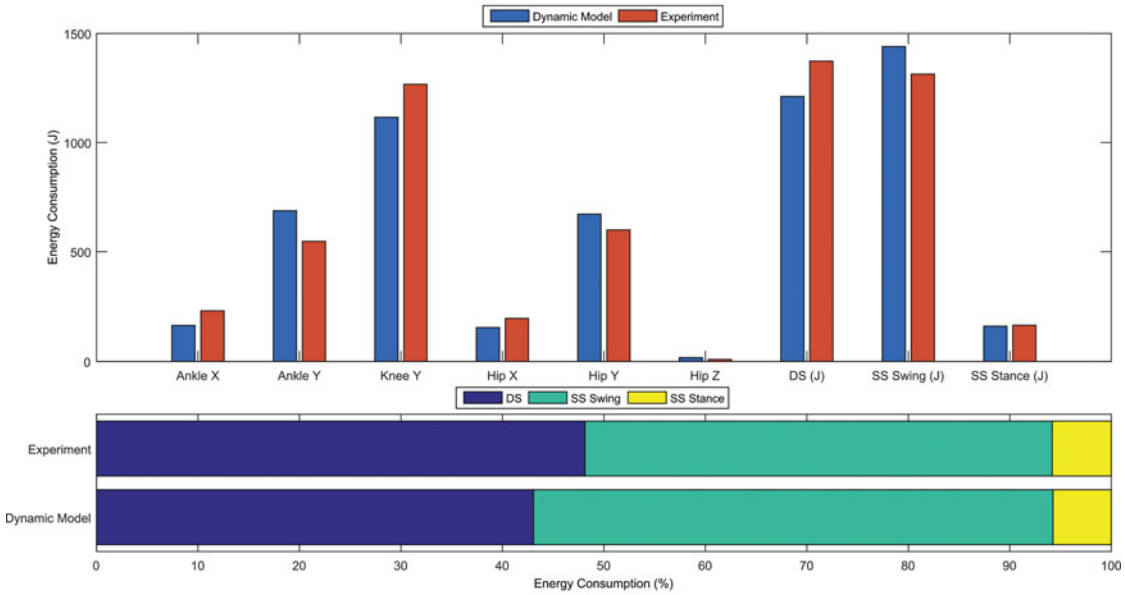


Fig. 9. Joint energy consumption of right foot based on the presented dynamic model and motor current.

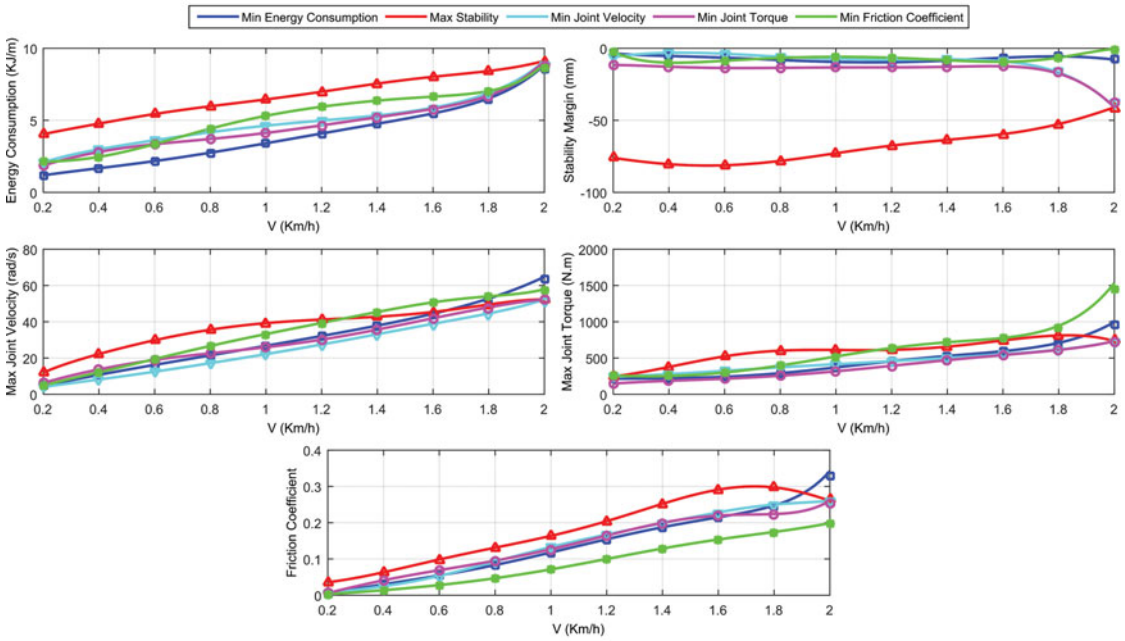


Fig. 10. Optimization results for the five goal functions with respect to robot velocity.

pattern which is optimized to have minimum energy consumption is lower than the other curves in all robot velocities.

As it can be seen in the second subplot, all optimization results have a small stability margin expect for the one in which maximum stability was the optimization target. It shows that these optimal gaits can be unstable in experimental tests. Therefore, it may be practical to have a minimum stability margin in optimization procedure. Moreover, it can be seen that by increasing the robot velocity, larger joint velocity, torque and friction coefficient are required.

To inspect effect of heel-strike and toe-off parameters more precisely, a parametric study is carried out to determine the effect of Q_{ff} (heel-strike angle) and Q_{fb} (toe-off angle). In this parametric study, Q_{ff} and Q_{fb} are considered to be fixed and other walking pattern parameters are optimized using GA.

https://doi.org/10.1017/S0263574718000140 Published online by Cambridge University Press

This process is repeated to sweep all feasible values for Q_{ff} and Q_{fb}. The results for walking velocity of 1.0 Km/h are depicted in Fig. 11.

The optimum results for minimum energy consumption and minimum required joint velocity and torque criteria are as follows:

$$\begin{aligned} \text{Min Energy Consumption} &\Rightarrow Q_{ff} = 17^\circ, \quad Q_{fb} = 12^\circ \\ \text{Min Joint Velocity} &\Rightarrow Q_{ff} = 12^\circ, \quad Q_{fb} = 17^\circ \\ \text{Min Joint Torque} &\Rightarrow Q_{ff} = 2^\circ, \quad Q_{fb} = 17^\circ \end{aligned} \tag{29}$$

This observation suggests that for each motion velocity, there exists an optimal Q_{ff} and Q_{fb} in which energy consumption and required joint velocity and torque are minimum.

Also, it can be assumed that by increasing Q_{fb}, stability of robot increases, while Q_{ff} does not have any influence on this criterion. This is due to the fact that the robot tends to tip over backward. This phenomenon also can be seen in Fig. 7 in which center of mass in X direction at the start of motion ($t = 0$) is close to the lower bound of support polygon (heel) rather than the upper bound (toe). Hence, toe-off motion with larger foot angle (Q_{fb}) improves total stability of the robot, while heel-strike motion does not affect that.

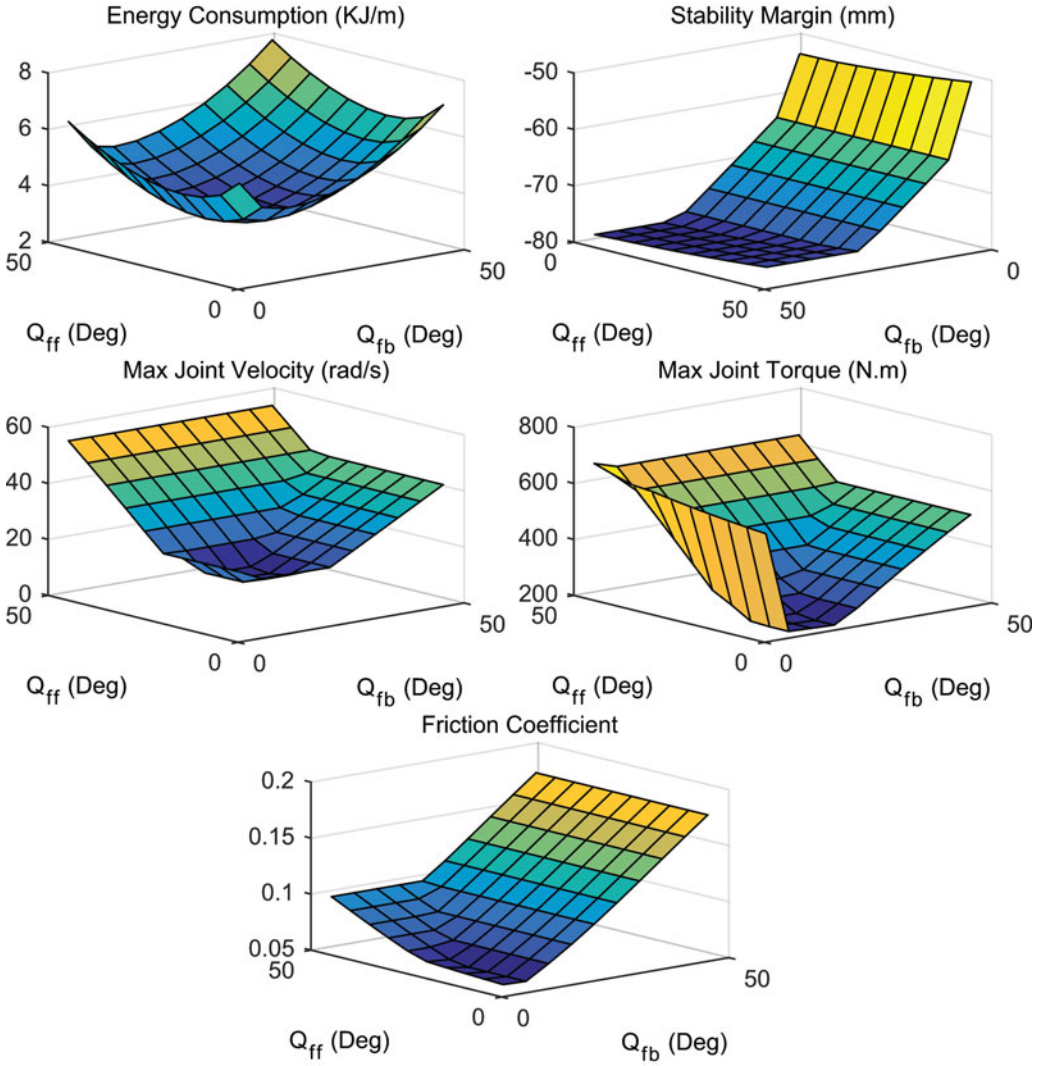


Fig. 11. Effect of Q_{ff} (heel-strike angle) and Q_{fb} (toe-off angle) on the optimization of goal functions.

https://doi.org/10.1017/S0263574718000140 Published online by Cambridge University Press

Another interesting observation is that heel-strike and toe-off motions with large foot angle increase the required friction coefficient. In other words, walking pattern without heel-strike and toe-off motions requires less friction coefficient than the one with heel-strike and toe-off motions. This is in compliance with human motion on slippery surfaces in which heel-strike and toe-off motions are avoided.[46,47]

Another parametric analysis is implemented to determine the effect of M_{toe} (toe mass) and L_{toe} (toe length) on goal functions. In this regard, several optimizations are carried out in which M_{toe} and L_{toe} varies from zero to $0.5M_{\text{foot}}$ and $0.5L_{\text{foot}}$, respectively. The results of these optimizations for walking velocity of 1.0 Km/h are depicted in Fig. 12.

It can be seen that by increasing M_{toe}, energy consumption and minimum torque criteria increase slightly. This is due to the fact that total mass of the robot increases. However, changes in L_{toe} does not affect goal functions.

Also, minimum velocity criterion is independent from M_{toe} and L_{toe}. The presented path planning method is based on robot kinematics. Therefore, it is rational that M_{toe} does not affect minimum velocity goal function. Moreover, ankle trajectories do not rely on L_{toe} (see Eqs. (10) and (11)). Hence, it is also reasonable that L_{toe} does not influence this goal function.

Another interesting observation is that by increasing M_{toe}, stability of motion increases and the required friction coefficient decreases as well. In other words, by using heavier toe link, probability of tip-over instability and slippage occurrence decreases. Also, L_{toe} does not affect these goal functions. It may be expected that by using larger support polygon, the stability of the robot will increase.

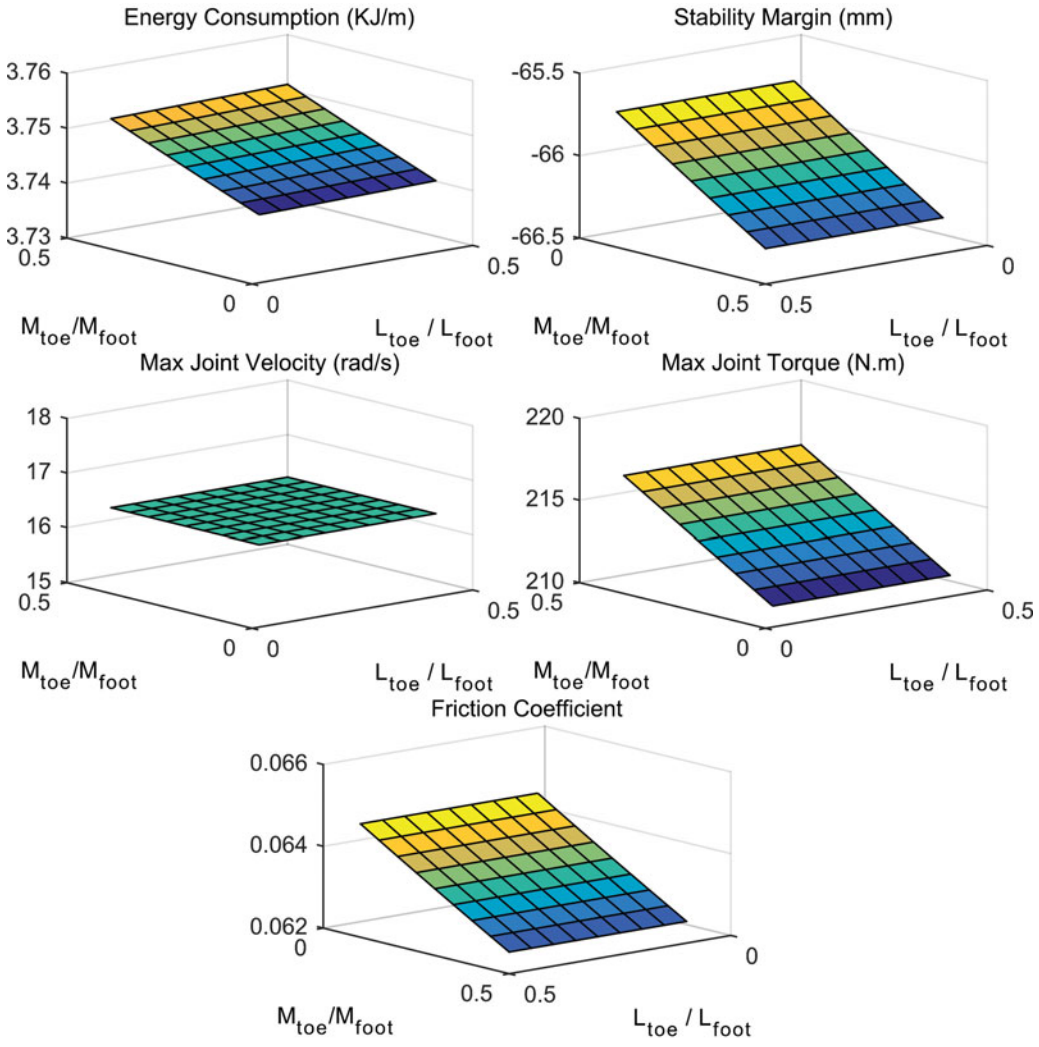


Fig. 12. Effect of M_{toe} (toe mass) and L_{toe} (toe length) on the optimization of goal functions.

https://doi.org/10.1017/S0263574718000140 Published online by Cambridge University Press

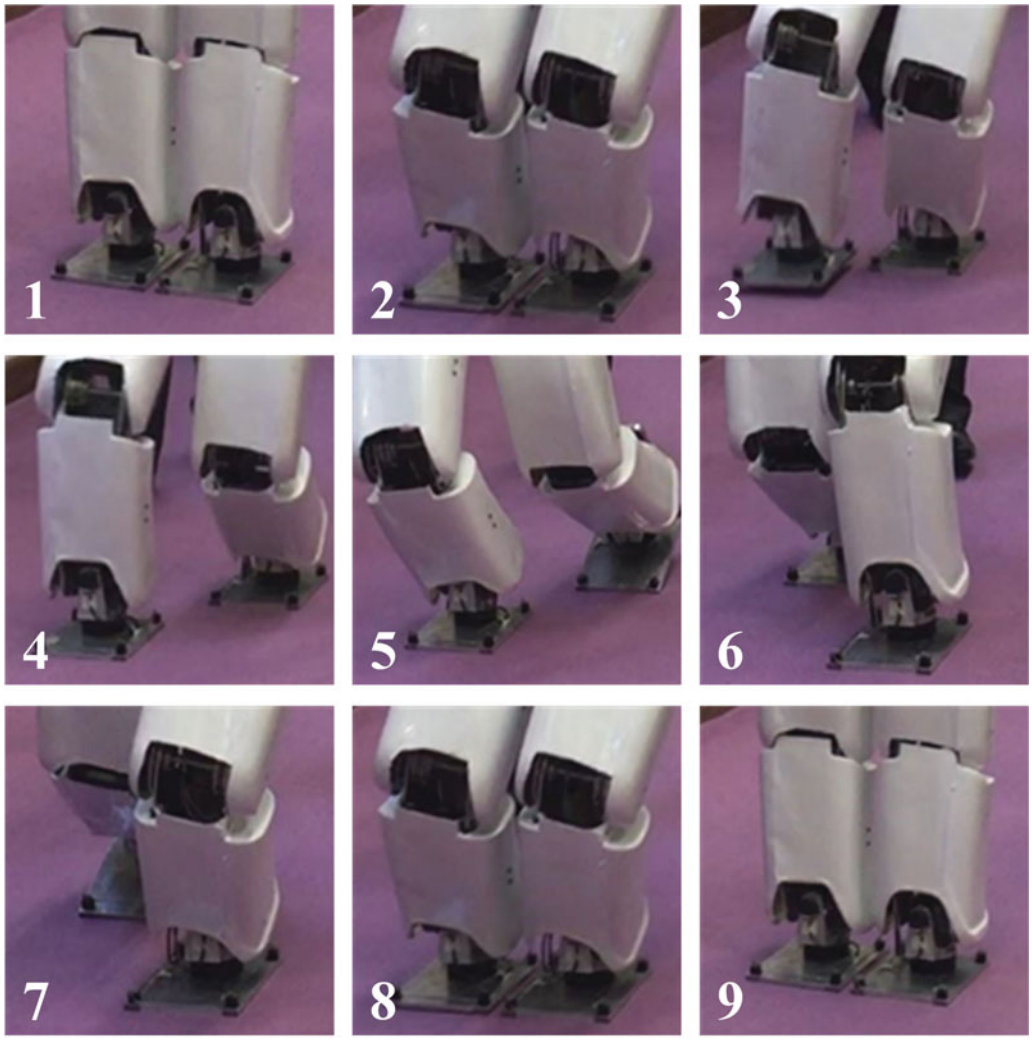


Fig. 13. Snapshots of experimental test of one cycle of gait with toe-off motion at the velocity of 0.7 Km/h.

However, as it was mentioned, robot tends to tip over backward, so larger toe link does not increase the stability of the motion.

In Fig. 13, snapshots of experimental test of one cycle of gait with toe-off motion at the velocity of 0.7 Km/h are illustrated.

6. Conclusion

In this paper, effects of heel-strike and toe-off motion parameters on walking pattern of a 3D humanoid robot equipped with active toe joint have been studied. To do so, dynamic modeling of the robot has been developed at first. The presented model consists of two parts: multi-body dynamics based on Lagrange and Kane methods and power transmission dynamics based on the system identification approach. Then, gait planning of the robot with heel-strike and toe-off motions based on position of ankle and hip joint and orientation of feet and pelvis link in the task space has been presented. Moreover, several simulations and experimental tests on SURENA III humanoid robot have been carried out. Afterwards, optimization procedure based on the GA has been adopted to determine the optimal results for five different goal functions including energy consumption, stability, joint velocity, joint torque and friction coefficient. At the end, parametric analyses have been carried out to study the effect of heel-strike and toe-off angle and toe link mass and length on these five goal functions. Some interesting results are listed as follows:

https://doi.org/10.1017/S0263574718000140 Published online by Cambridge University Press

- There exists an optimal Q_{ff} and Q_{fb} for energy consumption, joint velocity and torque criteria in each walking velocity.
- Increasing Q_{fb} helps avoiding backward tip-over instability.
- Increasing Q_{ff} and L_{toe} helps avoiding forward tip-over instability.
- Walking pattern without heel-strike and toe-off motions requires less friction coefficient.
- Heavier toe link yields less tip-over instability and slippage occurrence, but more energy consumption and joint torque.
- Joint velocity is independent from M_{toe} and L_{toe}.

The future work is dynamic modeling and gait optimizing of a humanoid robot with passive toe joint.

Acknowledgments
The authors would like to express deep gratitude to the Industrial Development and Renovation Organization of Iran (IDRO) and Iran National Science Foundation (INSF) for financial supports to develop the SURENA III humanoid robot. We further thank the members of the Center of Advanced Systems and Technologies (CAST) for their valuable participation in design and fabrication of SURENA III humanoid robot.

References

1. D. Tlalolini, C. Chevallereau and Y. Aoustin, "Comparison of different gaits with rotation of the feet for a planar biped," *Robot. Auton. Sys.* **57**, 371–383 (2009).
2. D. Tlalolini, C. Chevallereau and Y. Aoustin, "Human-like walking: Optimal motion of a bipedal robot with toe-rotation motion," *IEEE/ASME Trans. Mechatronics* **16**, 310–320 (2011).
3. J. Choi and J. Grizzle, "Planar Bipedal Walking with Foot Rotation," *Proceedings of the 2005 American Control Conference, (IEEE, 2005)*, pp. 4909–4916.
4. K. Nishiwaki, S. Kagami, Y. Kuniyoshi, M. Inaba and H. Inoue, "Toe Joints That Enhance Bipedal and Fullbody Motion of Humanoid Robots," *Proceedings of the ICRA'02, IEEE International Conference on Robotics and Automation, (IEEE, 2002)*, pp. 3105–3110.
5. T. Buschmann, S. Lohmeier and H. Ulbrich, "Humanoid robot lola: Design and walking control," *Physiology-Paris* **103**, 141–148 (2009).
6. R. Tajima, D. Honda and K. Suga, "Fast Running Experiments Involving a Humanoid Robot," *IEEE International Conference on Robotics and Automation, ICRA'09 (IEEE, 2009)*, pp. 1571–1576.
7. K. Miura, M. Morisawa, F. Kanehiro, S. Kajita, K. Kaneko and K. Yokoi, "Human-Like Walking with Toe Supporting for Humanoids," *IEEE/RSJ International Conference on Intelligent Robots and Systems (IROS), (IEEE, 2011)*, pp. 4428–4435.
8. Y. Ogura, K. Shimomura, A. Kondo, A. Morishima, T. Okubo, S. Momoki, H. Lim and A. Takanishi, "Human-Like Walking with Knee Stretched, Heel-Contact and Toe-Off Motion by a Humanoid Robot," *IEEE/RSJ International Conference on Intelligent Robots and Systems (IEEE, 2006)*, pp. 3976–3981.
9. P. Doubliez, O. Bruneau and F. Ouezdou, "Force control of the redundant leg of a biped robot to produce large inertial effects for crossing obstacles," *Int. J. Humanoid Robot.* **9**, 125–130 (2012).
10. A. Ki, L. Cheol and G. Jo, "Development of a Biped Robot with Toes to Improve Gait Pattern," *IEEE/ASME International Conference on Advanced Intelligent Mechatronics, (IEEE, 2003)*, pp. 729–734.
11. L. Wang, Z. Yu, Q. Meng and Z. Zhang, "Influence Analysis of Toe-Joint on Biped Gaits," *IEEE International Conference on Mechatronics and Automation, (IEEE, 2006)*, pp. 1631–1635.
12. E. Kouchaki and M. J. Sadigh, "Effect of Toe-Joint Bending on Biped Gait Performance," *IEEE International Conference on Robotics and Biomimetics (ROBIO), (IEEE, 2010)*, pp. 697–702.
13. N. Handharu, J. Yoon and G. Kim, "Gait Pattern Generation with Knee Stretch Motion for Biped Robot Using Toe and Heel Joints," *8th IEEE-RAS International Conference on Humanoids, (IEEE, 2008)*, pp. 265–270.
14. M. J. Sadigh, E. Kouchaki and C. Wu, "Effects of constraints on standing balance of a biped with toe-joints," *Int. J. Humanoid Robot.* **09**, 125–136 (2012).
15. R. Sellaouti, O. Stasse, S. Kajita, K. Yokoi and A. Kheddar, "Faster and Smoother Walking of Humanoid Hrp-2 with Passive Toe Joints," *IEEE/RSJ International Conference on Intelligent Robots and Systems, (IEEE, 2006)*, pp. 4909–4914.
16. S. Kajita, K. Kaneko, M. Morisawa, S. Nakaoka and H. Hirukawa, "Zmp-Based Biped Running Enhanced by Toe Springs," *IEEE International Conference on Robotics and Automation, (IEEE, 2007)*, pp. 3963–3969.
17. R. Kumar, N. Handharu, Y. Jungwon and K. Gap-soon, "Hybrid Toe and Heel Joints for Biped/Humanoid Robots for Natural Gait," *Proceeding of the ICCAS'07, International Conference on Control, Automation and Systems, (ICCAS, 2007)*, pp. 2687–2692.

https://doi.org/10.1017/S0263574718000140 Published online by Cambridge University Press

18. P. Channon, S. Hopkins and D. Pham, "Derivation of optimal walking motions for a bipedal walking robot," *Robotica* **10**, 165–172 (1992).
19. C. Chevallereau and Y. Aoustin, "Optimal reference trajectories for walking and running of a biped robot," *Robotica* **19**, 557–569 (2001).
20. V. Dau, C. Chew and A. Poo, "Achieving energy-efficient bipedal walking trajectory through ga-based optimization of key parameters," *Int. J. Humanoid Robot.* **6**, 609–629 (2009).
21. G. Capi, Y. Nasu, L. Barolli, K. Mitobe and K. Takeda, "Application of genetic algorithms for biped robot gait synthesis optimization during walking and going up-stairs," *Adv. Robot.* **15**, 675–694 (2001).
22. J. Park and M. Choi, "Generation of an optimal gait trajectory for biped robots using a genetic algorithm," *JSME Int. J. Ser. C Mech. Syst. Mach. Elements Manuf.* **47**, 715–721 (2004).
23. M. Rostami and G. Bessonnet, "Sagittal gait of a biped robot during the single support phase. Part 2: Optimal motion," *Robotica* **19**, 241–253 (2001).
24. G. Bessonnet, P. Seguin and P. Sardain, "A parametric optimization approach to walking pattern synthesis," *The Int. J. Robot. Res.* **24**, 523–536 (2005).
25. O. Kwon and J. Park, "Asymmetric trajectory generation and impedance control for running of biped robots," *Auton. Robots* **26**, 47–78 (2009).
26. S. Aoi and K. Tsuchiya, "Generation of bipedal walking through Interactions among the robot dynamics, the oscillator dynamics, and the environment: Stability characteristics of a five-link planar biped robot," *Auton. Robots* **30**, 123–141 (2011).
27. S. Aoi and K. Tsuchiya, "Locomotion control of a biped robot using nonlinear oscillators," *Auton. Robots* **19**, 219–232 (2005).
28. M. Sadedel, A. Yousefi-Koma and M. Khadiv, "Offline Path Planning, Dynamic Modeling and Gait Optimization of a 2d Humanoid Robot," *2nd RSI/ISM International Conference on Robotics and Mechatronics (ICRoM), (IEEE, 2014)*, pp. 131–136.
29. M. Khadiv, S. A. Moosavian and M. Sadedel, "Dynamics Modeling of Fully-Actuated Humanoids with General Robot-Environment Interaction," *2nd RSI/ISM International Conference on Robotics and Mechatronics (ICRoM), (IEEE, 2014)*, pp. 233–238.
30. B. Ugurlu, J. Saglia, N. Tsagarakis and D. Caldwell, "Yaw moment compensation for bipedal robots via intrinsic angular momentum constraint," *Int. J. Humanoid Robot.* **9**, 1250033 (2012).
31. G. Carbone, Y. Ogura, H. Lim, A. Takanishi and M. Ceccarelli, "Dynamic simulation and experiments for the design of a new 7-dofs biped walking leg module," *Robotica* **22**, 41–50 (2004).
32. T. Wang, C. Chevallereau and C. Rengifo, "Walking and steering control for a 3d biped robot considering ground contact and stability," *Robot. Auton. Syst.* **60**, 962–977 (2012).
33. Y. Aoustin and A. Formalskii, "3d walking biped: Optimal swing of the arms," *Multibody Syst. Dyn.* **32**, 55–66 (2014).
34. S. Kajita and K. Tani, "Study of Dynamic Biped Locomotion on Rugged Terrain-Derivation and Application of the Linear Inverted Pendulum Mode," *Proceedings of the 1991 IEEE International Conference on Robotics and Automation, (IEEE, 1991)*, pp. 1405–1411.
35. S. Kajita, F. Kanehiro, K. Kaneko, K. Fujiwara, K. Harada, K. Yokoi and H. Hirukawa, "Biped Walking Pattern Generation by Using Preview Control of Zero-Moment Point," *Proceedings of the ICRA'03. IEEE International Conference on Robotics and Automation, (IEEE, 2003)*, pp. 1620–1626.
36. J. Park and K. Kim, "Biped Robot Walking Using Gravity-Compensated Inverted Pendulum Mode and Computed Torque Control," *Proceedings. 1998 IEEE International Conference on Robotics and Automation, (IEEE, 1998)*, pp. 3528–3533.
37. T. Sato, S. Sakaino and K. Ohnishi, "Real-time walking trajectory generation method with three-mass models at constant body height for three-dimensional biped robots," *IEEE Trans. Ind. Electron.* **58**, 376–383 (2011).
38. Q. Huang, K. Yokoi, S. Kajita, K. Kaneko, H. Arai, N. Koyachi and K. Tanie, "Planning walking patterns for a biped robot," *IEEE Trans. Robot. Autom.* **17**, 280–289 (2001).
39. H. Baruh, *Analytical Dynamics* (WCB/McGraw-Hill, Boston, 1999).
40. M. Vukobratović and B. Borovac, "Zero-moment point-thirty five years of its life," *Int. J. Humanoid Robot.* **1**, 157–173 (2004).
41. J. Grcar, "How ordinary elimination became gaussian elimination," *Historia Math*. **38**, 163–218 (2011).
42. A. Ben and T. Greville, *Generalized Inverses: Theory and Applications*, vol. 15 (Springer Science & Business Media, 2003).
43. H. Taghirad and P. Belanger, "Modeling and parameter identification of harmonic drive systems," *J. Dyn. Syst. Meas. Control, Trans.-Am. Soc. Mech. Eng.* **120**, 439–444 (1998).
44. J. Nunez, A. Briseno, D. Rodriguez, J. Ibarra and V. Rodriguez, "Explicit Analytic Solution for Inverse Kinematics of Bioloid Humanoid Robot," *Robotics Symposium and Latin American Robotics Symposium (SBR-LARS), (IEEE, 2012)*, pp. 33–38.
45. Q. Huang and Y. Nakamura, "Sensory reflex control for humanoid walking," *IEEE Trans. Robot.* **21**, 977–984 (2005).
46. W. Hsu, T. Wang, H. Lu and T. Lu, "Anticipatory changes in control of swing foot and lower limb joints when walking onto a moving surface traveling at constant speed," *Gait and Posture* **41**, 185–191 (2015).
47. R. Cham and M. Redfern, "Changes in gait when anticipating slippery floors," *Gait and Posture* **15**, 159–171 (2002).

https://doi.org/10.1017/S0263574718000140 Published online by Cambridge University Press